Comparative study of intermetallic phases formed by direct ion implantation and radiation enhanced diffusion of tin in two kinds of steel

P. H. Dionisio, B. A. S. de Barros Jr., and I. J. R. Baumvol

Citation: Journal of Applied Physics **58**, 773 (1985); doi: 10.1063/1.336195
View online: http://dx.doi.org/10.1063/1.336195
View Table of Contents: http://scitation.aip.org/content/aip/journal/jap/58/2?ver=pdfcov
Published by the AIP Publishing

Comparative study of intermetallic phases formed by direct ion implantation and radiation enhanced diffusion of tin in two kinds of steel

P. H. Dionisio, B. A. S. de Barros, Jr., and I. J. R. Baumvol
Instituto de Física, Universidade Federal do Rio Grande do Sul, 90000 Porto Alegre, RS, Brasil

(Received 16 October 1984; accepted for publication 22 January 1985)

The surface layers of high-carbon and stainless steel samples, treated by both direct ion implantation of Sn^+ ions and radiation enhanced diffusion of tin, are analyzed by means of Rutherford backscattering and ^{119}Sn and ^{57}Fe conversion electron Mössbauer spectroscopy. The intermetallic phases formed in the treated surfaces are determined and their thermal evolution is established. The compositions and phase transformations observed in the surfaces of the samples treated by both direct ion implantation and radiation-enhanced diffusion are very similar, and this similarity indicates that these two treatment processes are essentially equivalent for practical applications.

I. INTRODUCTION

The introduction of tin atoms into the surface layers of iron and steels by means of direct ion implantation has been reported by many authors as responsible for significant modifications of the tribological and high-temperature oxidation behavior of these materials.[1–5] These improvements were associated with the formation of intermetallic compounds during implantation. Second phase precipitates like $FeSn_2$, FeSn, and Ni_3Sn_2 can account for hardening as well as for the enhancement on the elastic limit of the tin-implanted surfaces.[6] The improvement of the high-temperature oxidation properties of tin-implanted pure iron was associated,[4] by analogy with tinplating, with the intermetallic compound $FeSn_2$, which acts as a barrier between the active iron substrate and the oxidizing environment, greatly reducing the surface area of the iron that is sacrificially protected by SnO_2.[7] Oxidative wear is also influenced by this mechanism.[1,3]

These facts indicated the importance of identifying the phases formed on the surface of iron and steels when implanted with tin and their relative proportions, as well as the transformations they undergo when submitted to temperatures typical of the practical working conditions. Such a knowledge is essential for the understanding of mechanisms responsible for the protective effects that are observed and also in predicting new applications.

In a previous publication, we showed the results of our investigations on the surface composition of pure iron, carbon steel, and stainless steel implanted with Sn^+ ions.[8] The technique used to identify the phases formed in the surfaces of these substrates, when implanted with doses of 1×10^{17} Sn^+ cm^{-2} at 200 keV, and their thermal evolution was the following:

(i) ^{119}Sn conversion electron Mössbauer spectroscopy (CEMS) analysis was performed on the as-implanted surfaces. The components used to fit the CEMS spectra were identified by comparison with data from the literature on transmission Mössbauer spectroscopy of stoichiometric intermetallic compounds.

(ii) The samples from (i) were annealed in high vacuum at temperatures in the range 200–900 °C. After every annealing temperature, a ^{119}Sn CEMS spectrum was recorded. By comparing the new parameters for each component of the fitting with the Mössbauer data from the literature, we could establish the phase transformations occurring at the surface of the samples.

(iii) The phase transformation schemes obtained in this way were then compared with the phase diagrams for the Fe-Sn and Ni-Sn systems. This comparison allowed, in most cases, an unambiguous determination of the kind of precipitates formed during implantation and their thermal evolution.

Ion beam mixing (IBM) or radiation-enhanced diffusion (RED) as an alternative method to treat metallic surfaces for tribological and corrosion purposes is now being increasingly used,[9,10] since the high cost of direct implantation of heavy metallic species is one of the major obstacles for its industrial utilization.

In the present work, we extend the phase determination method described above to the case of ion beam mixing or radiation-enhanced diffusion of tin into the surface layers of the same high carbon and stainless steels already studied for direct ion implantation coating. We used here both ^{119}Sn and ^{57}Fe CEMS in order to identify the intermetallic compounds formed when a thin film of Sn is bombarded with energetic Ar^+ ions. The details of the experimental conditions are given in Sec. II. The interest on the kind of work reported is to investigate whether the same phases are formed by ion beam mixing as in direct Sn^+ implantation. If this is so, then all the beneficial effects of ion implantation of tin into steels could be also obtained by ion beam mixing.

The idea of using ion beam mixing comes from the recoil implantation technique.[10] Recoil implantation can be used to introduce dopant atoms into a substrate. A thin layer of the desired dopant is deposited on the substrate surface and bombarded with energetic ions. The range of the ions must be at least comparable with the initial thickness of the deposited overlayer. Kinetic energy is transferred to the atoms in the overlayer, some of which come to rest into the substrate.

A considerable advantage of recoil implantation is the relative simplicity of the technique. A beam of ions of an

 0021-8979/85/140773-06$02.40

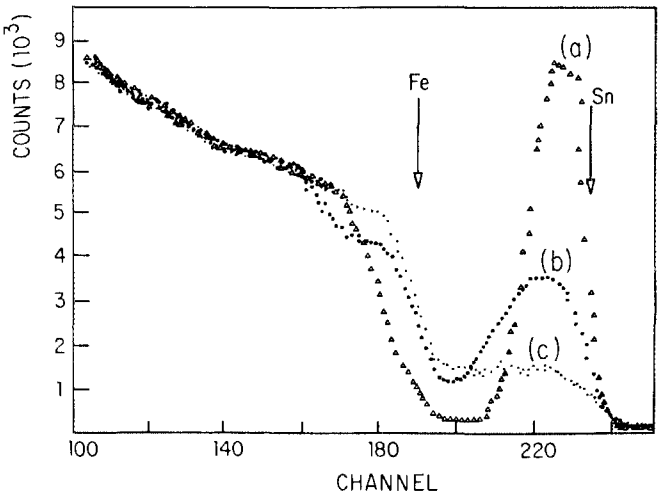

FIG. 1. RBS of 760-keV α particles for a stainless steel sample: (a) evaporated with a 600-Å tin film, (b) after bombardment with 1×10^{17} cm^{-2}, 300-keV Ar^+ ions, and (c) after bombardment and annealing in high vacuum at 800 °C during 1 h.

inert gas is usually used, and any element that can be deposited in thin layers ($\sim$100 Å) can be implanted. The main disadvantage of recoil implantation is the very shallow depth to which material can be implanted. This can be overcome by a subsequent thermal diffusion, but for many applications, the high temperatures required have disadvantages, apart from the energy costs involved in high-temperature treatment. The required temperature can be reduced by exploiting radiation-enhanced diffusion, as it is now clear that at a given temperature the diffusion coefficient can be enhanced by several orders of magnitude.[11–13] The increased vacancy concentration due to the irradiation causes a proportional increase in diffusion by the vacancy mechanism; in addition, substitutional atoms are ejected into interstitial sites, from which they diffuse rapidly. These two transport processes comprise what is usually called radiation-enhanced diffusion. The overall atomic diffusivity under conditions of radiation-enhanced diffusion is governed by the production rate of mobile vacancies and interstitials, by the mobility of these defects, and by the probabilities of their annihilation by recombination, agglomeration, or assimilation into immobile sinks. The main driving force for the redistribution process comes not from classical random walk diffusion, but from the solute flow biased either with or against the defect flow, depending on the kind of moving defects and the kind of interaction (attractive or repulsive) between these defects and the solute atoms. The in-diffusion reported in the present work is the net result of the contributions to the solute flow given by each one of these competitive processes.

II. EXPERIMENTAL DETAILS AND RESULTS

A. Experimental details

Samples of a high carbon tool steel (1C, 0.5Cr, 1.2Mn, 0.5W) and 18/8/1 stainless steel (0.15C, 18Cr, 8Ni, 2Mn) were mechanically and electrolytically polished. The samples were evaporated with tin films with an estimated thickness of 600 Å in a vacuum of 10^{-5} Pa and then bombarded with 300-keV Ar^+ ions, to a dose of 1×10^{17} cm^{-2}. The temperature of the samples during bombardment were always kept below 300 °C and the Ar^+ flux was 5 μA cm^{-2}.

The depth profiles of the diffused Sn atoms were determined by means of Rutherford backscattering (RBS) measurements, using 760-keV $^4He^{++}$ ions in normal incidence, detecting the scattered particles at an angle of 160° with the direction of incidence. The energy resolution of the detection system was 14 keV.

All the Ar^+ bombardments and RBS measurements were performed at the 400-keV High-Voltage Engineering Europa ion implanter (HVEE-400) at Institute of Physics, Porto Alegre.

The CEMS spectra were obtained in a backscattering geometry. Experimental details, as well as the data reduction and analysis procedures, can be obtained in Refs. 8 and 14–16. Sources for the CEMS measurements were ^{119m}Sn in $BaSnO_3$ and ^{57}Co in Rh. The isomer shifts δ are quoted with respect to $BaSnO_3$ and to pure iron in each case.

To study the thermal evolution of the phases formed during bombardment, the samples were annealed in a vacuum of 10^{-5} Pa at temperatures progressively higher in the range from 300 to 900 °C during 1 h.

B. RBS measurements

In Fig. 1, we show typical RBS spectra for a stainless steel sample evaporated with a 600-Å tin film [Fig. 1(a)], for this sample bombarded with 1×10^{17} cm^{-2}, 300-keV Ar^+ ions [Fig. 1(b)], and finally for the bombarded sample after annealing in high vacuum at 800 °C during 1 h [Fig. 1(c)].

Figure 1(b) reveals clearly the amount of tin atoms diffused into the surface layers of the stainless steel substrate. Also, the backward sputtering of the tin atoms from the film

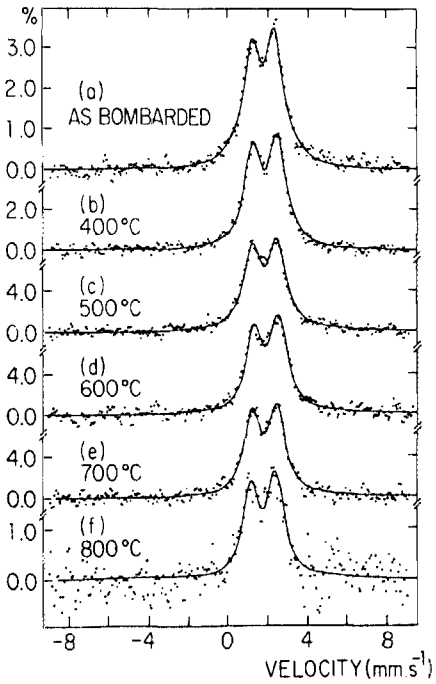

FIG. 2. ^{119}Sn CEMS spectra for the stainless steel sample treated by RED, as bombarded and after annealing in high vacuum at various temperatures (see text and Table I).

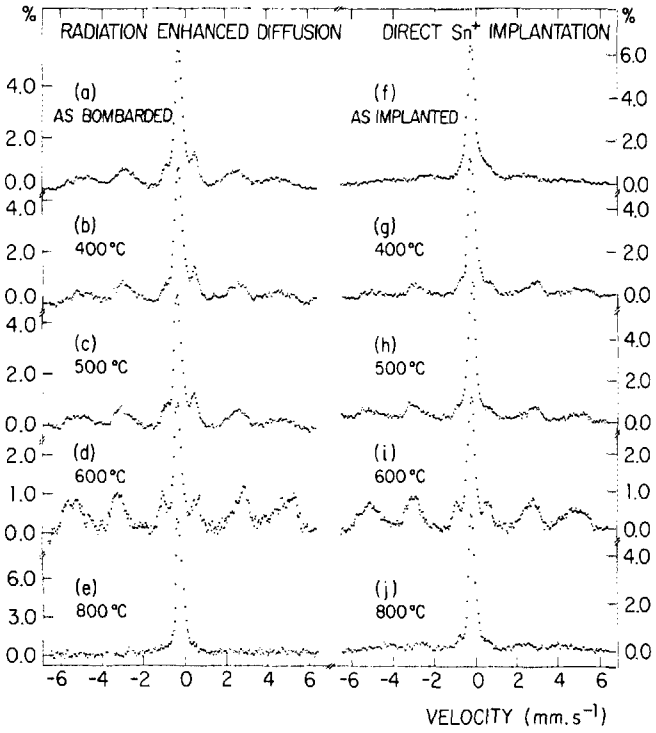

FIG. 3. ^{57}Fe CEMS spectra for the stainless steel samples, as treated and after annealing in high vacuum at various temperatures: (a)–(e) sample treated by RED; (f)–(j) sample treated by direct ion implantation (see text and Table II).

is revealed by the reduction in area of the RBS spectrum corresponding to scattering from Sn nuclei.

In Fig. 1(c), we can see the pronounced loss of Sn from the surface layers, due to both thermal in-diffusion of the already radiation-enhanced diffused Sn atoms and the evaporation of Sn due to the high annealing temperature.

The situation shown in Fig. 1 is very characteristic of all the carbon and stainless steel samples. The only difference was that the loss of tin from the surfaces due to evaporation or in-diffusion into deeper regions of the carbon steel substrates occurred at a much lower annealing temperature than in the stainless steel substrates.

C. CEMS analysis

In Fig. 2, we show the ^{119}Sn CEMS spectra for the stainless steel sample treated by RED. The lines through the data points are least-square fits to the experimental points. All these spectra were fitted with only one doublet (see Table I) whose Mössbauer parameters are very close to those associated with the intermetallic compound Ni_3Sn_2,[6,8,17–19] although there is a marked asymmetry in the intensity of the lines. Such an asymmetry is also reported in Ref. 6 for an Fe-Ni-Sn alloy. Small discrepancies in fitting the external parts of the doublets are due to small proportions of Fe-Sn phases. These results are very similar to those obtained for directly implanted samples,[8] with the difference that in that case the CEMS analysis revealed the presence of larger amounts of Fe-Sn phases at the lower annealing temperatures.

In Figs. 3(a) to 3(e), we show the ^{57}Fe CEMS spectra for the same RED treated sample of Fig. 2. In addition to the central paramagnetic singlet, characteristic of the stainless steel substrate, we identify contributions to the spectra due to large distributions of magnetic hyperfine fields that change significantly as we increase the annealing temperature. These spectra have been analyzed by the usual Mössbauer computer data reduction procedure called "stripping," as exemplified in Fig. 4. In Fig. 4(a), we repeat the spectrum from Fig. 3(d); the full line represents the best fitting to the stainless steel peak only. Figure 4(b) represents the spectrum resulting from the subtraction of the full line from the experimental points in Fig. 4(a); now, here in Fig. 4(b), the full line represents the best fitting to the spectrum so generated. The same kind of subtraction procedure in Fig. 4(b), giving rise to Fig. 4(c), shows that there are no significant components remaining from the original spectrum. In the process of fitting the field distributions like that appearing in Fig. 4(b), we usually limited ourselves to five sextets representing one hyperfine magnetic field each.

We interpret the magnetic part of our ^{57}Fe CEMS spectra obtained for the radiation enhanced diffused stainless steel sample as resulting from a substitutional solid solution of impurity atoms in the iron matrix. By doing so, we identified each sextet as resulting from a magnetic hyperfine field $H(m,n)$ on an ^{57}Fe nucleus having m impurity atoms at the first near-neighbor sphere and n impurity atoms at the second near-neighbor sphere and we tabulated the following quantities:

$$H(0,0),$$
$$\Delta H_1 = H(0,0) - H(1,0),$$
$$\Delta H_2 = H(0,0) - H(0,1),$$
$$H_r = \Sigma_{ij} H(i,j) A_{ij}.$$

The values of ΔH_1 and ΔH_2 were obtained under the assumption that $H(m,n) = H(0,0) - m\Delta H_1 - n\Delta H_2$, which implies the additivity of the effects of the neighboring impurity atoms. The A_{ij} are the relative contributions of the $H(i,j)$ components to the magnetic part of the spectrum and were obtained from the intensity and width of the resonance lines, which were used as fitting parameters. Our definition of H_r is analogous to that currently used in the literature,[20,21] with A_{ij} in place of p_{ij}, the probability of an ^{57}Fe atom being in the neighboring configuration (i,j) in the alloy. It is reasonable to suppose that A_{ij} is proportional to p_{ij}, so that our values of H_r can be compared with those quoted in the literature. The

TABLE I. Mössbauer parameters from the fitting of the doublets in the ^{119}Sn CEMS spectra for the stainless steel samples treated by RED. Isomer shifts are given relative to SnO_2.

Annealing temperature (°C)	ΔE_Q (mm/s ± 0.05)	δ (mm/s ± 0.08)	Γ (mm/s ± 0.03)
RT	1.05	1.73	1.00
400	1.23	1.81	1.00
500	1.23	1.81	1.00
600	1.24	1.78	0.95
700	1.21	1.76	0.93
800	1.23	1.72	1.00

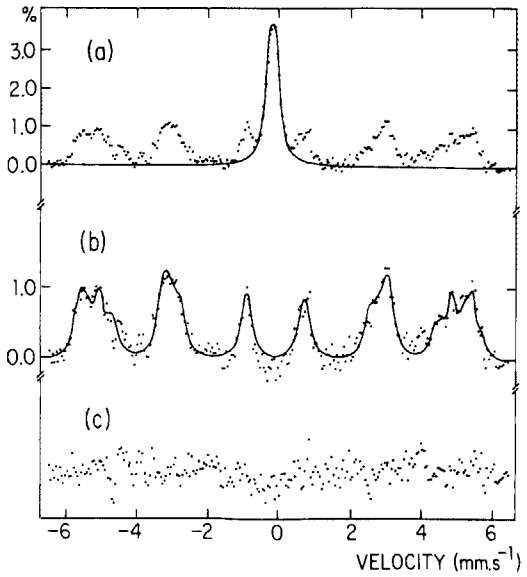

FIG. 4. ^{57}Fe CEMS spectrum for the stainless steel sample treated by RED and annealed in high vacuum at 600 °C: (a) the original experimental spectrum (points) and the best fitting to the stainless steel peak (full line), (b) after subtracting the stainless steel peak from the experimental spectrum (points) and the best fitting to the hyperfine magnetic fields (full line), and (c) after a new subtraction performed on (b) (see text and Table II).

results presented in the upper half of Table II agree very well with those reported for solid solutions of Cr in Fe,[20,21] where similar values of $H(0,0)$ and H_r were obtained for chromium concentrations of about 10–15 at. %. The contribution of those fields to the whole spectrum increases with the annealing temperature up to above 600 °C, then decreasing and practically disappearing at 800 °C.

In Figs. 3(f) to 3(j) and in the lower half of Table II, we show the corresponding results for the sample directly implanted with Sn^+ ions. The behavior is very similar to the one corresponding to the samples treated by RED, although it was impossible to decide between the two sets of values presented for ΔH_1 and ΔH_2 at 500 and 600 °C. Moreover, the contribution of large magnetic fields to the spectrum seems more significant at 800 °C.

The ^{119}Sn CEMS spectra for the NSOH tool steel sample treated by RED and annealed at various temperatures are displayed in Fig. 5(a). The parameters from the least-square fittings are given in Table III. The fitting procedure is exemplified in Fig. 5(b). Firstly, a doublet of $\Delta E_Q = 1.46$ mm/s and a magnetic hyperfine field of $H = 34$ kOe indicate the presence of the intermetallic compound FeSn[8,22,23]; the presence of such a magnetic hyperfine field is much less apparent in the spectrum taken in bulk for a stoichiometric and homogeneous sample at room temperature as shown in Ref. 22. The third component, with $H = 25$ kOe and $\delta = 2.00$, is related to the presence of $FeSn_2$.[8,23–25] Finally, broad distributions of large hyperfine magnetic fields are interpreted as solid solutions of tin in iron at concentration around 2.5 at. %.[8,23,26] Table III shows that the presence of $FeSn_2$ diminishes with increasing annealing temperature and disappears completely at 500 °C, while the intermetallic FeSn and the solid solution increase their contribution. Annealing at 600 °C results in a very poorly defined spectrum with a small absorption coefficient where only the presence of a very dilute solid solution is apparent. This behavior is again similar to one of the directly implanted samples as described in Ref. 8, with minor differences: the relative contribution of $FeSn_2$ to the total area of the spectra is smaller, the temperatures at which $FeSn_2$ and FeSn decompose are lower, and the temperature at which the surface layer starts to loose tin is also lower. Repeated efforts to confirm these observations by ^{57}Fe CEMS measurements both for RED and directly implanted samples were not successful; this is most probably because the proportions of intermetallic phases formed in tool steel were too small to produce enough absorption to distinguish them from the magnetic contributions from the substrate due to its martensitic structure.

III. DISCUSSIONS AND CONCLUSIONS

The thermal evolution of the compounds formed by radiation-enhanced diffusion of tin into carbon and stainless steels can be compared with the phase diagrams for the Fe-Sn, Ni-Sn and Cr-Sn systems.[27–32] From Refs. 30–32, we know that the Ni_3Sn_2 intermetallic is stable up to 1264 °C. In our stainless steel sample, we observed that Ni_3Sn_2 is still stable at 900 °C, although there is an evident loss of tin from

TABLE II. Parameters obtained from the fitting of the ^{57}Fe CEMS spectra of the stainless steel samples. Figures in parentheses represent alternative possible values.

Sample treatment	Annealing temperature (°C)	$H(0,0)$ (kOe ± 3)	ΔH_1 (kOe ± 6)	ΔH_2 (kOe ± 6)	H_r (kOe ± 6)
RED	RT	336	34	22	307
	400	340	40	25	307
	500	338	32	24	312
	600	342	33	18	314
	800		not fitted		
Direct Sn^+ implantation	RT		not fitted		
	400	345	36	25	309
	500	345	33(20)	20(13)	314
	600	346	33(23)	23(14)	310
	800		not fitted		

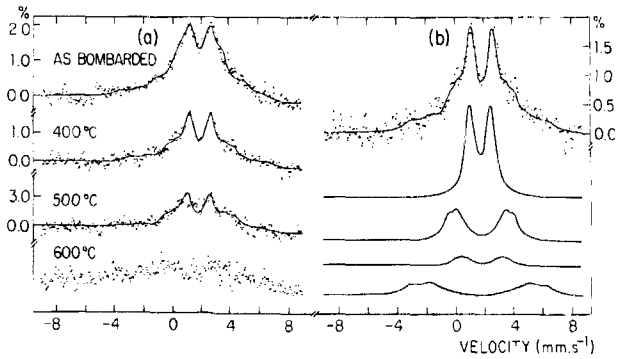

FIG. 5. (a) ^{119}Sn CEMS spectra for the NSOH tool steel sample treated by RED, as bombarded and after annealing in high vacuum at various temperatures, (b) the spectrum after annealing at 400 °C is repeated with the components obtained from the fitting (see text and Table III).

the surface at this temperature. This means that the phase Ni_3Sn_2 formed in the surface layers of the stainless steel substrate by means of RED, starts to decompose at a lower temperature than that quoted in the phase diagram for the Ni-Sn system in bulk.

Exactly the same tendency is shown by the intermetallics $FeSn_2$ and FeSn. In the Fe-Sn phase diagram we see that $FeSn_2$ decomposes at 498 °C, giving FeSn and free Sn. Here in our samples we can already observe its incipient decomposition at 400 °C. The FeSn intermetallic, on the other hand, should be stable up to 740 °C, whereas it is seen to start its decomposition around 600 °C in the RED carbon steel sample.

This behavior can be understood if we consider that we are dealing here with nonstoichiometric, heavily damaged, nonbinary systems. Moreover, as it has been reported by several authors,[33,34] the precipitates formed during ion bombardment are usually very finely dispersed, with grain sizes ranging between 20 and 200 Å. The fine dispersion of the intermetallic precipitates appears to be the reason for its earlier decomposition. Previous work with carbonitride precipitates formed by N^+ implantation into steels has widely confirmed this interpretation.[35] Another possible cause for the dissolution of the intermetallic phases, at temperatures lower than those quoted in the respective phase diagrams, is the depletion in the Sn concentration that we observe in the CEMS spectra as the annealing temperature is increased. We comment on this effect also below in connection with the discussion of the Fe-Cr solid solutions.

TABLE III. Mössbauer parameters from the fitting of the ^{119}Sn CEMS spectra for the carbon steel samples treated by RED. Isomer shifts are given with respect to SnO_2. Figures in parentheses represent the error in the last significant figure.

Annealing temperature (°C)	H (kOe)	ΔE_Q (mm/s)	δ (mm/s)	Γ (mm/s)	Relative area (%)	Phase
RT	...	1.48(4)	1.88(3)	0.85	42	FeSn
	35(3)	...	1.98(3)	0.86	26	
	25(2)	...	2.00(2)	0.84	15	$FeSn_2$
	71(4)	...	1.68(8)	1.30	17	*Fe*Sn
400	...	1.46(3)	1.95(2)	0.83	47	FeSn
	34(3)	...	1.98(3)	0.84	28	
	25(2)	...	2.00(2)	0.84	4	$FeSn_2$
	68(4)	...	1.82(6)	1.30	21	*Fe*Sn
500	...	1.53(3)	1.86(2)	0.90	46	FeSn
	35(3)		2.00(3)	0.84	31	
	71(3)	...	1.44(4)	1.30	23	*Fe*Sn
600	Not fitted					

With these peculiarities in mind, we can say that the phase decomposition schemes obtained in the present work essentially confirm the phase diagrams for Fe-Sn and Ni-Sn intermetallics, thus supporting the given interpretations for the CEMS spectra of the various samples here analyzed.

Another comparison can be established between the present results and those obtained in our previous work[8] from direct implantation of Sn^+ ions. There is a great similarity in the CEMS spectra, both for ^{119}Sn and ^{57}Fe, measured for the stainless steel samples treated by direct implantation and RED. This can be clearly seen when one compares Fig. 2 and Table I of the present work with Fig. 4 and Table II from Ref. 8 (^{119}Sn data), as well as the left half with the right half of Fig. 3, and the upper half with the lower half of Table II (^{57}Fe data).

One comment is necessary concerning the solid solution of Cr in Fe as observed by ^{57}Fe CEMS in stainless steel. There is an appreciable uncertainty in the determination of the parameters quoted in Table II and some of the magnetic components in each spectrum could perhaps have a different interpretation; especially in the cases of the implanted samples annealed at 500 and 600 °C, the alternative values of 20 and 13 kOe found for ΔH_1 and ΔH_2, respectively, would be in accordance with those reported in Ref. 26 for *Fe*Sn solid solutions. We have identified all the magnetic contributions in the ^{57}Fe spectra for stainless steel as due to *Fe*Cr solid solutions based on thermal decomposition arguments: the ^{119}Sn spectra show that the surface layers of the samples are being cleaned up of Fe-Sn intermetallics as the annealing temperature increases, while the ^{57}Fe spectra show increasing contributions of the components ascribed to the *Fe*Cr solid solution. We conclude then that Ni is being progressively precipitated in the form of the Ni_3Sn_2 compound, leaving the remaining Fe and Cr atoms from the original stainless steel composition free to form the *Fe*Cr substitutional solid solution. The annealing at even higher temperatures (800 °C and above) confirms this picture, since the loss of Sn from the surface, following the precocious decomposition of Ni_3Sn_2, releases again the Ni atoms to rebuild the paramagnetic structure of stainless steel. It is known that the presence of Ni stabilizes stainless steel in its austenitic character, reflected in the ^{57}Fe CEMS spectrum by the single central line (see Figs. 3 and 4).

In the case of high-carbon steel samples, we notice the same pronounced similarity between the intermetallic phases formed through direct Sn^+ implantation and radiation-enhanced diffusion of tin. This is revealed by comparing Fig. 5 and Table III of the present work with Fig. 3 and Table II of Ref. 8. There are, however, minor differences between the relative proportions and decomposition tem-

peratures for the $FeSn_2$ and FeSn intermetallics that could perhaps be investigated in further detail.

The overall similarity in the surface composition of the Sn^+ ion implanted samples and those radiation enhanced diffused with tin indicates that the same beneficial effects on the tribological and high-temperature oxidation behavior of metallic components can be accomplished by RED as well as by direct implantation. Indeed, not only the direct implantation of Sn^+ ions into iron, titanium, carbon, and stainless steel has shown to reduce drastically the wear rate of these materials,[1-5] but also RED of tin proved to be equally beneficial.[36,37] It is interesting at this point to compare our results on stainless steel to those reported by Calliari *et al.*[19]; those authors obtained Ni_3Sn and Ni_3Sn_2 by ion beam mixing a tin film deposited on a Ni substrate and verified that this treatment substantially increases the tarnishing resistance of nickel. Moreover, in a recent observation of the high-temperature oxidation properties of carbon steel implanted with Sn^+ and radiation-enhanced diffused with tin, we observed that both methods are very effective in reducing the oxidation rate. All these facts support the idea that second phase precipitates such as $FeSn_2$, FeSn, and Ni_3Sn_2 play an important role on the improvement of the surface mechanical, tribological, and high-temperature properties of metal and steels treated by ionic bombardment.

ACKNOWLEDGMENTS

We are grateful to our colleagues F. C. Zawislak, P. J. Viccaro, W. H. Schreiner, and C. A. dos Santos for the careful reading of the manuscript. This work was supported in part by Financiadora de Estudos e Projetos (FINEP), Coordenação do Aperfeiçoamento do Pessoal de Nível Superior (CAPES) and Conselho Nacional de Desenvolvimento Científico e Tecnológico (CNPq), Brasil.

[1] I. J. R. Baumvol, R. E. J. Watkins, G. Longworth, and G. Dearnaley, Inst. Phys. Conf. Ser. **54**, 201 (1980).
[2] R. E. S. Watkins, AERE-Harwell, Internal Report (1980).
[3] I. J. R. Baumvol, G. Longworth, L. W. Becker, and R. E. J. Watkins, Hyperf. Interac. **10**, 1123 (1981).
[4] I. J. R. Baumvol, J. Appl. Phys. **52**, 4583 (1981).
[5] E. B. Hale, M. M. Muehlemann, W. Baker, and R. A. Kosher, in "Proceedings of the NATO Advanced Study Institute on Surface Engineering," Preliminary copy, Les Arcs, France (1983).
[6] Z. Eliezer, B. Z. Weiss, M. Ron, and S. Nadiv, J. Appl. Phys. **44**, 419 (1973).
[7] H. Leidheiser, Jr., *The Corrosion of Copper, Tin and Their Alloys* (Wiley, New York, 1971).
[8] P. H. Dionisio, B. A. S. de Barros, Jr., and I. J. R. Baumvol, J. Appl. Phys. **55**, 4219 (1984).
[9] A. Galerie and G. Dearnaley, Nucl. Instrum. Methods **209/210**, 823 (1983).
[10] J. P. Gaillard, in "Proceedings of the NATO Advanced Study Institute on Surface Engineering," Preliminary copy, Les Arcs, France (1983).
[11] G. J. Dienes and A. C. Damask, J. Appl. Phys. **29**, 1713 (1958).
[12] R. L. Minear, D. G. Nelson, and J. F. Gibbons, J. Appl. Phys. **43**, 3468 (1972).
[13] S. M. Myers, D. E. Amos, and D. K. Brice, J. Appl. Phys. **47**, 1812 (1976).
[14] M. J. Tricker, in "Mössbauer Spectroscopy and Its Chemical Applications," edited by J. G. Stevens and G. K. Shenoy, Adv. Chem. Ser. **194**, 63 (1981).
[15] G. Longworth and R. Atkinson, in "Mössbauer Spectroscopy and Its Chemical Applications," edited by J. G. Stevens and G. K. Shenoy, Adv. Chem. Ser. **194**, 101 (1981).
[16] G. P. Huffman and F. E. Huggins, in "Mössbauer Spectroscopy and Its Chemical Applications," edited by J. G. Stevens and G. K. Shenoy, Adv. Chem. Ser. **194**, 265 (1981).
[17] H. Z. Dokuzogus, L. H. Bowen, and H. H. Stadelmaier, J. Phys. Chem. Solids **31**, 1565 (1970).
[18] J. Silver, C. A. Mackay, and J. D. Donaldson, J. Mater. Sci. **11**, 836 (1976).
[19] L. Calliari, L. M. Gratton, L. Guzman, G. Principi, and C. Tosello, presented at the Symposium on Ion Implantation and Ion Beam Processing of Materials, Annual Meeting of the MRS, Boston, 1983.
[20] S. M. Dubiel, J. Żukrowski, J. Korecki, and K. Krop, Acta Phys. Pol. **A47**, 199 (1975).
[21] S. M. Dubiel, Acta Phys. Pol. **A49**, 619 (1976).
[22] C. Djéga-Mariadassou, P. Lecocq, G. Trumpy, J. Träff, and P. Østergaard, Nuovo Cimento, **XLVI B**, 35 (1966).
[23] G. Trumpy, E. Both, C. Djéga-Mariadassou, and P. Lecocq, Phys. Rev. B **2**, 3477 (1970).
[24] V. I. Nikolaiev, Yu. I. Shcherbina, and S. S. Yakimov, J. Exp. Theoret. Phys. (USSR) **45**, 1277 (1963).
[25] G. P. Huffman and G. R. Dunmyre, J. Electrochem. Soc. **125**, 1652 (1978).
[26] I. Vincze and A. T. Aldred, Phys. Rev. B **9**, 3845 (1974).
[27] C. A. Edwards and A. Preece, J. Iron Steel Instrum. **124**, 41 (1931).
[28] W. F. Ehret and A. F. Westgren, J. Am. Chem. Soc. **55**, 1339 (1933).
[29] W. D. Jones and W. E. Hoare, J. Iron Steel Instrum. **129**, 273 (1934).
[30] M. Hausen, *Constitution of Binary Alloys* (McGraw-Hill, New York, 1958).
[31] R. P. Elliot, *Constitution of Binary Alloys*, lst Supplement (McGraw-Hill, New York, 1965).
[32] F. A. Shunk, *Constitution of Binary Alloys, 2nd Supplement* (McGraw-Hill, New York, 1969).
[33] H. Herman, Nucl. Instrum. Methods **182/183**, 887 (1981).
[34] C. A. dos Santos, B. A. S. de Barros, Jr., J. P. de Souza, and I. J. R. Baumvol, Appl. Phys. Lett. **41**, 237 (1982).
[35] C. A. dos Santos, M. Behar, and I. J. R. Baumvol, J. Phys. D **17**, 551 (1984).
[36] I. J. R. Baumvol, Phys. Status Solidi A **67**, 287 (1981).
[37] L. Guzman and I. Scotoni, in "Proceedings of the NATO Advanced Study Institute on Surface Engineering," Preliminary copy, Les Arcs, France (1983).